Synthesis of Twisted [*N*]Cycloparaphenylenes by Alkene Insertion

Tomoaki Terabayashi,[†] Eiichi Kayahara,*,[†] Yoshiyuki Mizuhata,[†] Norihiro Tokitoh,[†] Toru Nishinaga,[‡] Tatsuhisa Kato,[†] and Shigeru Yamago*,[†]

[†]Institute for Chemical Research, Kyoto University, Uji 611-0011, Japan

[‡]Department of Chemistry, Tokyo Metropolitan University, Hachioji, Tokyo 192-0397, Japan

ABSTRACT: Mono- and bis-alkene-inserted [*N*]cycloparaphenylenes (CPPs) **1** and **3** (abbreviated as (ene)-[*N*]CPP and (ene)$_2$-[*N*]CPP, respectively; *N* = 6, 8, and 10) and mono *ortho*-phenylene-inserted [6]CPP **2** were synthesized by fusing CPP precursors and alkene or *ortho*-phenylene groups via coupling reactions. Single-crystal X-ray diffraction (XRD) analyses reveal that rotation of the paraphenylene units in **1**, **2**, and **3** is suppressed in the solid phase and that the stripes formed by the π-surfaces of **1** and **2** exhibit a Möbius topology. In contrast, while a doubly twisted structure is possible for **3**, it exhibits a Hückel topology in the crystalline state. The twist is localized near the alkene moiety, with the angle between the alkene and neighboring paraphenylene unit being 30-54° for **1** and ~70° for **3**. Despite the significant twisting angle, **1** has in-plane conjugation with a quinoidal contribution, as determined by XRD analysis, Raman spectra, and theoretical calculations. In contrast, the in-plane conjugation is quite limited in **3**. The absorption and fluorescence spectra of **1** and **3** show opposite size dependencies; redshifts and blueshifts occur for **1** and **3**, respectively, as the size decreases. These results are consistent with the size dependence of the HOMO-LUMO energy gap; the HOMO and LUMO energies increase and decrease, respectively, as the size of **1** decreases, and this is the second example after CPPs showing this unusual electronic property. In contrast, the HOMO and LUMO energies decrease and increase, respectively, as the size of **3** decreases, which is typical. The oxidation potential also shows opposite size dependency between **1** and **3**; it decreases as the size of **1** decreases, as predicted from the HOMO energy. The introduction of an alkene group in the CPP moiety in **1** and **3** significantly relieves the molecular strain compared to that of the parent CPPs, but these are still highly strained molecules, particularly **1**. The strain energy of **1** is >100 kJ mol^{-1}, and the strain is localized at the paraphenylene unit located farthest from the alkene group. This localization of the strain is the origin of the instability of the radical cation of **1**, which undergoes dimerization initiated at the most strained paraphenylene unit.

Since the discovery of fullerenes[1] and carbon nanotubes (CNTs),[2] curved cyclic π-conjugated molecules with in-plane π-orbitals have attracted significant attention as synthetic targets due to their unique structure and potential applications in materials science.[3] An in-plane Hückel π-conjugated molecule can be formally synthesized by joining both ends of a normal (linear) ·-conjugated molecule, and twisting the normal π-conjugated molecules before joining the ends can formally yield a Möbius molecule (Figure 1a). However, these synthetic strategies have never been realized due to the difficulty of directly converting a linear molecule to a cyclic molecule.

Two alternative synthetic strategies to prepare Möbius molecules are currently known. One strategy is to combine a Hückel molecule with in-plane π-orbitals and a normal π-conjugated molecule, as proposed by Herges and realized by fusing tetradehydrodianthracene and [*n*]annulene.[4, 5] The other synthetic strategy is to connect a partially twisted π-conjugated molecule in a cyclic structure, and various Möbius molecules consisting of expanded porphyrins,[6-9] binaphthyl,[10] helicenes,[11] and substituted phenanthrenes[12] have already been synthesized. Despite these developments, however, the structural variety and synthetic methods of Möbius molecules are still limited. Furthermore, while twisting in a Möbius molecule would significantly alter the properties of a Hückel molecule, elucidation of the physical properties has also been limited.

We report here a new synthetic method to prepare Möbius molecules using the characteristic structure of [*N*]cycloparaphenylenes
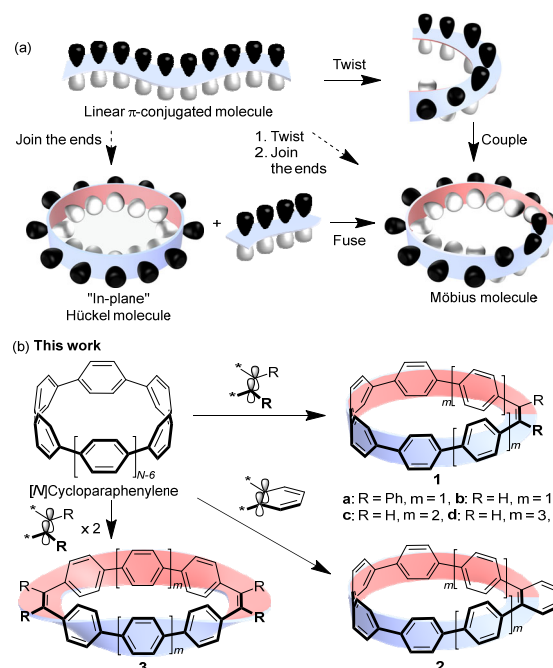

Figure 1. Schematic illustration of (a) the concepts for synthesizing Hückel and Möbius molecules and (b) this work.

([N]CPPs, Figure 1b),[13-15] which have the shortest sidewall segments of armchair CNTs with in-plane π-orbitals. We envisioned that the insertion of alkene or ortho-phenylene units, which have a normal π-structure, into the paraphenylene units in CPP would yield Möbius molecules (Figure 1b). Here, we report a proof of principle for the synthesis of alkene- and ortho-phenylene-inserted [6]-, [8]-, and [10]CPPs, which are abbreviated as ene-[N]CPP (1) and phe-[N]CPP (2), respectively, and studied their structures and physical properties. We also synthesized bis-alkene-inserted [N]CPP 3, which is abbreviated as (ene)2-[N]CPP, to clarify the effect of twisting on the molecular structure and physical properties.

Meta-phenylene-inserted CPPs have previously been synthesized,[16] but the meta-substituted unit is cross-conjugated to the CPP moiety. In contrast, as ortho-phenylene- and alkene-inserted CPPs can be fully conjugated, the degree of in-plane conjugation of ene [N]CPPs and phe-(N)CPPs is of great interest. Additionally, the synthesis of phe-[6]CPP[17] and (phe)2-[6]CPP[18] has previously been reported, but the topological properties and size dependency have not yet been studied. Furthermore, three examples of the synthesis of CPP derivatives with Möbius topology have recently been reported: CPPs twisted by structural restriction caused by tethers[19] and figure-eight-shaped CPPs with bicarbazole spirobifluorene units as the twisting groups.[20, 21] However, the method described here has never previously been reported.

We found that 1 and 2 adopt a Möbius structure in the solid phase and exhibit in-plane conjugation despite significant twisting. Furthermore, 1 possesses a unique dependence of the electronic properties on size; specifically, the HOMO-LUMO energy gap decreases as the size of the phenylene unit decreases. The observed size dependence is the same as that observed in CPPs[22] but opposite to that observed in conventional linear π-conjugated oligomers. Therefore, ene-CPPs are the second example of this unique inverse HOMO-LUMO dependence on size. In contrast, 3 exhibits a Hückel topology in a solid phase and follows the conventional HOMO-LUMO dependency on size.

RESULTS AND DISCUSSION

Synthesis. The synthesis of diphenyl-ene-[6]CPP 1a (R = Ph, m = 1) began with a twofold Suzuki-Miyaura coupling reaction between (Z)-1,2-bis(pinacolatoboryl)stilbene 4[23] and three-ring unit 5,[24] which was used in previous CPP syntheses (Scheme 1a). The coupling reaction selectively took place at the iodine group of 5, affording dibromide 6a in 40% yield. Then, a Ni(0)-mediated homocoupling reaction of 6a afforded cyclic product 7a in 54% yield. The reductive aromatization of the diyl moieties in 7a by H2SnCl4[24] afforded 1a in 86% yield.

The parent ene-[6]CPP 1b, ene-[8]CPP 1c, and ene-[10]CPP 1d (R = H, m = 1, 2, and 3) were synthesized by extending the synthetic method used for the synthesis of 1a starting from cis-1,2-bis(4-bromophenyl)ethene (8bA, X = Br).[25] Transmetallation to the lithium salt (X = Li) and subsequent reaction with ketone 9 followed by triethylsilyl protection afforded 6b in 48% yield. Treatment of the same lithium species with iPrOBpin afforded 8bB, which underwent twofold Suzuki-Miyaura coupling with 5, providing 6c in excellent yields. Furthermore, the same twofold Suzuki-Miyara coupling starting from 8cB, which was synthesized by the homologation of 8bB, gave 6d in good combined yields. Ni(0)-mediated intramolecular coupling and reductive aromatization afforded 1b, 1c, and 1d in high overall yields. The method was scalable, and 0.5 and 0.4 g of 1b and 1c were obtained, respectively. Phe-[6]CPP 2 was also synthesized starting from 1,2-bis(pinacolatoboryl)benzene 10 using the same synthetic procedure used for 1 (Scheme 1b).

(Ene)2-[N]CPP 3 (N = 6 and 8) was also synthesized by platinum-mediated dimerization of linear precursors, which was used for the synthesis of CPPs (Scheme 1c).[26] For example, treatment of bis-borated cis-alkene 11B synthesized from bromide 11A with Pt(cod)Cl2 (cod = 1,5-cyclooctadiene, 1.0 equiv) in the presence of K3PO4 (5.0 equiv) in THF at 65 °C afforded bis-platinum complex 12b. Subsequent reductive elimination of platinum from 12b gave 3b (m = 1, N = 6) in 25% yield (2 steps). Starting from 8cB, 3c (m = 2, N = 8) was synthesized in 44% yield (2 steps).

Scheme 1. Selective synthesis of 1, 2, and 3.
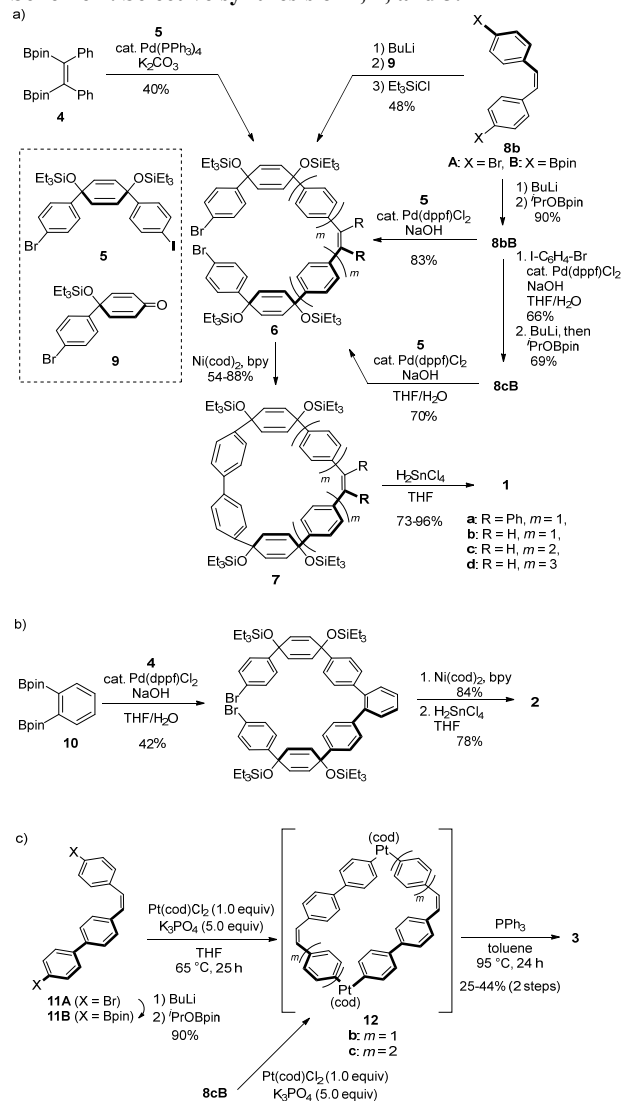
Structural Analysis. The structures of 1 and 2 were initially estimated by NMR in CDCl3 at 25 °C. In the ^{1}H NMR spectrum of 1b, protons of the alkene appear as a singlet, and those of the paraphenylene rings appear as six doublets. The results suggest that the paraphenylene unit freely rotates at room temperature within the timescale of the NMR measurement. In the ^{13}C NMR spectrum, twelve peaks corresponding to the carbon atoms of the paraphenylene units and one signal corresponding to the alkene were detected. All these spectra are consistent with the C2v symmetric structure of 1b in solution. All ene-[N]CPPs (1a, 1c, and 1d) and phe-[6]CPPs 2 also have C2v symmetric structures in solution.

In the ^{1}H NMR spectrum of (ene)$_2$-[6]CPP **3b**, protons of the alkene appeared as singlets, and those of the terphenyl units appeared as one singlet and two doublets. In the ^{13}C NMR spectrum, 3 quaternary and 4 methine carbons were detected. These observations suggest that **3b** adopts a D_{2h} symmetric structure in solution. **3c** also adopts the D_{2h} structure in solution.

MALDI-TOF mass spectrometry of all the compounds showed the desired molecular ion mass, further supporting the successful synthesis of **1**, **2**, and **3**.

The structures of **1**, **2**, and **3** were unambiguously determined by single-crystal X-ray diffraction (XRD) analysis of crystals of **1a-d**, **2**, and **3b** (Figures 2a-f). For **1a**, the crystal belongs to the monoclinic $P2_1/n$ space group and contains a pair of enantiomers in each unit cell (Figure 2a). **1a** adopts C_2 symmetry, in which the symmetry axis passes through the center of the alkene and the facing C_{ipso}-C_{ipso} bond of the paraphenylene units *C* and *C'*. In sharp contrast to the structure of **1a** in solution, the paraphenylene unit is frozen and does not rotate in the crystalline structure. Therefore, the inside and outside of the π-surface can be defined and can be traced with a single knotless string. This result suggests the Möbius topology of **1a**. The XRD analyses of **1b-d** and **2** also reveal that all molecules exhibit Möbius topology with frozen paraphenylene units in crystalline form.
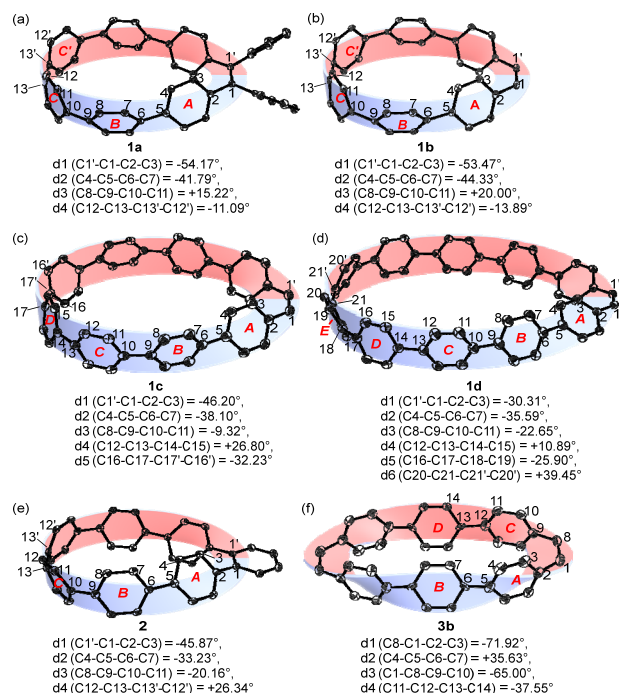

Figure 2. X-ray crystal structures of (a) **1a**, (b) **1b**, (c) **1c**, (d) **1d**, (e) **2**, and (f) **3b**. (*M*)-**1** isomer in the crystal of *rac*-**1** is shown. Paraphenylene units and carbon atoms are labeled in italics in red alphabetically and numbered in black according to the molecular symmetry. Dihedral angles (*d*n, n = 1-5) between the two paraphenylene units or alkene and paraphenylene unit A are highlighted in blue. Hydrogen atoms and solvents are omitted for clarity. The thermal ellipsoids are scaled at the 50% probability level.

The twist is localized at the alkene and adjacent rings A and B of the paraphenylene moiety. For example, the dihedral angles d1 (C1'-C1-C2-C3) and d2 (C4-C5-C6-C7) of **1a** are -53.27° and -44.33°, respectively, while those of d3 (C8-C9-C10-C11) and d4 (C12-C13-C13'-C12') are 15.22° and -11.09°, respectively (Figure

2a). The same trends are also observed for **1b-d** and **2**, in which dihedral angles d1 and d2 are significantly larger than other dihedral angles (Figure 2b-e).

The crystal of **3b** belongs to the tetragonal crystal system in the $P1$ space group (Figure 2f). **3b** has a C_s symmetric structure with a Hückel topology, as it has a mirror plane perpendicular to the hoop and passing through the center of rings B and D. Both alkene-ring *A* and alkene-ring *C* are highly distorted with dihedral angles d1 (C8-C1-C2-C3) and d3 (C1-C8-C9-C10) of -71.92° and -65.00°, respectively. In contrast, dihedral angles d2 (C4-C5-C6-C7) and d4 (C11-C12-C13-C14) are +35.63° and -37.55°, respectively, which are very similar to those of linear oligoparaphenylene.[22]

Strained structures of **1** and **2** are suggested from the shallow boat conformation of all paraphenylene units with two *ipso* carbons lying above the mean plane defined by the four *ortho* carbons. The out-of-plane bending angles of **1a** increase as the paraphenylene unit moves away from the alkene moiety [ring A (3.7 and 2.4° on C2 and C5), ring B (8.6 and 9.3° on C6 and C9), and ring C (14.3 and 15.1° on C10 and C13)]. This observation suggests that ring C is the most strained, followed by ring B, and ring A is the least strained. The bending angle of ring C is very similar to that of [5]CPP(15.6°),[27] and the angle of ring B is similar to that of small CPPs ([6]CPP = 12.7°,[28] [7]CPP =10.8°,[29] and [8]CPP = 9.6°).[30] These results suggest that the strain accumulates more in paraphenylene unit C, which is located farthest from the alkene group. Similar structural features are observed for **1b-d** and **2** (Table S9). On the other hand, the out-of-plane bending angles of **3b** were at most 5.0° (5.0° on C2 and C9, 4.6° on C5 and C12, and 2.9° on C6 and C13), and the results are consistent with the lower strain of **3** than of **1** and **2** (see below).

The contribution of the quinoidal form, **1'**, albeit a small amount, was suggested by bond length alternation (BLA) analysis, where BLA is defined as the difference between C_{ipso}-C_{ortho} and C_{ortho}-C_{ortho} bond lengths in the phenylene unit in Å (Table 1). For example, the BLA values of rings *A*, *B*, and *C* in **1a** are 0.012, 0.016, and 0.017 Å, respectively, suggesting a decrease and increase in the double bond character of the C_{ipso}-C_{ortho} bond and the C_{ortho}-C_{ortho} bond, respectively. The same degree of BLA was observed for **1b-d**, **2**, and **3b**, and these values are very similar to those observed in CPPs (0.015-0.017 Å).[31] However, these BLA values are significantly smaller than, for example, those of polyacetylenes (~0.03-0.05 Å).[32, 33] Therefore, the contribution of **1'** is relatively small, and this conclusion is consistent with the negligible effect on the C-C bond length of the alkene (1.330 Å) and C_{ipso}-C_{ipso} bonds (1.494 Å) in **1** and **3b**.

Table 1. Effect of Structure on the BLA (Å).

Compound	ring *A*	ring *B*	ring *C*	ring *D*	ring *E*
1a	0.011	0.016	0.022		
1b	0.012	0.016	0.017		
1c	0.015	0.019	0.015	0.018	
1d	0.009	0.015	0.009	0.017	0.017
2	0.012	0.016	0.019		
3b	0.012	0.015	0.012	0.015	

[a]BLA = bond length alteration, defined as the difference between the C_{ipso}-C_{ortho} and C_{ortho}-C_{ortho} bond lengths.
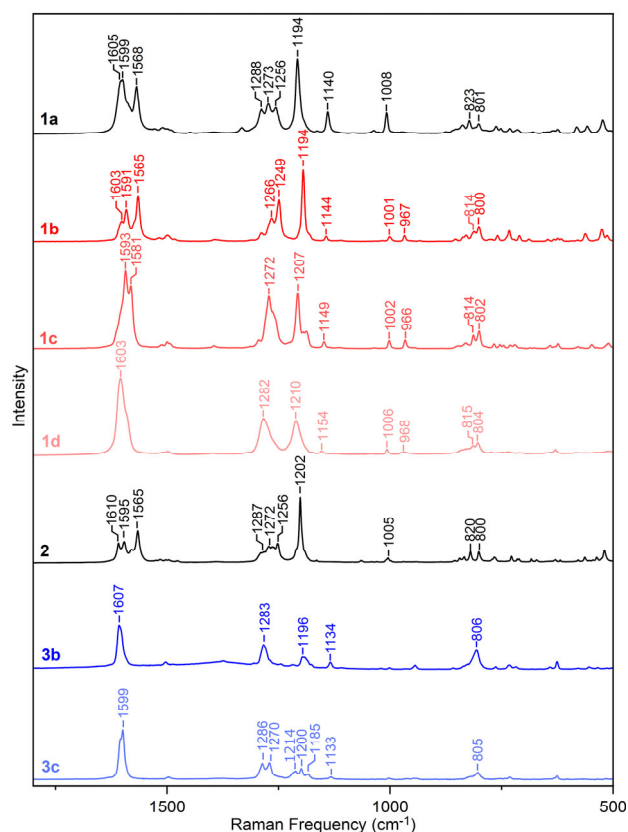
Figure 3. Raman spectra of solids 1, 2, and 3 using an excitation wavelength of 785 nm.

Despite being slight, the contribution of the quinoidal structure was also clearly observed in the Raman spectra of the solid samples

of **1**, **2**, and **3** (Figure 3). All samples showed strong bands at 1530-1700, 1320-1220, and 1210-1100 cm^{-1}, which were assigned as intra-ring C–C stretching ($\nu_{\text{intra-CC}}$), inter-ring C–C stretching ($\nu_{\text{inter-CC}}$), and in-plane C–H bending (δ_{CH}) modes, respectively, according to the density functional theory (DFT) calculation at the B3LYP/6-31G* level of theory (see the Supporting Information). The strong bands were shifted by up to 15 cm^{-1} to higher wave numbers as the ring size increased from **1b-1d**, suggesting an increased quinoidal contribution as the ring size decreased.[31] Weak bands observed at 1010–950, 750–850, and 550–500 cm^{-1} are attributable to out-of-plane deformations. On the other hand, the Raman bands of **3** exhibit the opposite size dependence on $\nu_{\text{intra-CC}}$ and $\nu_{\text{inter-CC}}$ modes relative to those of **1**, suggesting that the quinoidal contribution increases as the ring size of **3** increases.

Theoretical calculations. The optimized structures of **1a**, ene-[*N*]CPPs (*N* = 5-12), including **1b-d** (*N* = 6, 8, and 10, respectively), and **2** determined by DFT calculations at B3LYP/6-31G* have similar structural characteristics, i.e., the presence of a localized twist at the alkene moiety, a quinoidal contribution, and a shallow boat conformation of all paraphenylene units, in which paraphenylene units farther from the alkene lead to larger out-of-plane bending of the *ipso* carbons. The calculated structures of **1a-d** and **2** are very similar to those obtained by XRD analyses. The *trans* isomers of **1a**, **1b**, **1c**, and **1d** are 123, 75, 58, and 45 kJ mol^{-1} thermodynamically less stable than the corresponding *cis*-isomers, respectively. Therefore, isomerization to the *trans* isomer is unlikely.

The calculation of (ene)$_2$-[*N*]CPPs (*N* = 5-12), including **3b** (*N* = 6) and **3c** (*N* = 8), reveals the presence of several rotational isomers; the most stable conformation of **3b**, **3c**, (ene)$_2$-[10]CPP, and (ene)$_2$-[12]CPP is D_2, D_2, C_{2h}, and C_i symmetry, respectively, and that of odd (ene)$_2$-[*N*]CPPs is C_1 symmetry (See Tables S9). For **3b**, the D_2 symmetric isomer is 1.7 kJ mol^{-1} and 15 kJ mol^{-1} more stable

Table 2. Summary of the physical properties of 1-3, ene-[*N*]CPP, and (ene)$_2$-[*N*]CPP.

Molecule	Calculation[a]				Experimental					
	Strain energy (kJ mol^{-1})	HOMO (eV)	LUMO (eV)	HOMO-LUMO gap (eV)	λ_1 (nm)[b]	λ_2 (nm)[b]	HOMO-LUMO gap (eV)[b,c]	λ_{em} (nm)[b]	Φ_F[b]	E_{ox} (V) vs. Fc/Fc[+d,e]
Diphenyl-ene-[6]CPP (**1a**)	253	-4.97	-1.68	3.29	420	329	2.95 (2.41)	550	0.02	0.57
ene-[5]CPP	305	-4.90	-1.73	3.17	-	-	-	-	-	-
ene-[6]CPP (**1b**)	262	-5.06	-1.62	3.44	416	319	2.98 (2.53)	520		
ene-[7]CPP	227	-5.11	-1.64	3.47	-	-	-	-	-	-
ene-[8]CPP (**1c**)	199	-5.14	-1.67	3.47	383	328	3.24 (2.72)	483	0.59	0.68
ene-[9]CPP	179	-5.20	-1.62	3.58	-	-	-	-	-	-
ene-[10]CPP (**1d**)	160	-5.24	-1.60	3.64	379	330	3.27 (2.84)	462	0.84	0.78
ene-[11]CPP	157	-5.21	-1.65	3.56	-	-	-	-	-	-
ene-[12]CPP	138	-5.27	-1.60	3.67	-	-	-	-	-	-
phe-[6]CPP (**2**)	252	-5.06	-1.60	3.46	413	321	3.00 (2.55)	519	0.19	0.56
(ene)$_2$-[5]CPP	127	-5.35	-1.32	4.03	-	-	-	-	-	-
(ene)$_2$-[6]CPP (**3b**)	91	-5.29	-1.38	3.91	319	281	3.89 (3.38)	409, 424	0.25	0.97
(ene)$_2$-[7]CPP	90	-5.28	-1.46	3.82	-	-	-	-	-	-
(ene)$_2$-[8]CPP (**3c**)	74	-5.21	-1.58	3.63	348	310	3.56 (3.11)	419, 434	0.36	0.92
(ene)$_2$-[9]CPP	69	-5.26	-1.54	3.72	-	-	-	-	-	-
(ene)$_2$-[10]CPP	55	-5.27	-1.54	3.73	-	-	-	-	-	-
(ene)$_2$-[11]CPP	56	-5.25	-1.60	3.65	-	-	-	-	-	-
(ene)$_2$-[12]CPP	51	-5.26	-1.60	3.66	-	-	-	-	-	-

[a]The values were obtained from DFT calculations at the B3LYP/6-31G* level of theory. [b]Measured in CH_2Cl_2. [c]The values were obtained from the observed λ_1 values. The values in parentheses were obtained from the onset of the absorption spectra. [d]First oxidation potential. [e]The values were obtained from DPV measurements in $Bu_4NPF_6/(CH_2Cl)_2$ at room temperature.

than the C_{2h} and C_s symmetric isomers, respectively. The results are in sharp contrast to the observed C_s symmetric structure in the solid phase, but this difference is probably due to the effects of crystal packing forces and/or inclusion of solvent molecules. As the D_2 point group symmetry is a chiral group, **3b** can have an axial chirality with a double twisted structure, while C_{2h} and C_s point group symmetries are achiral groups. The results suggest that the chiral, doubly twisted structure can be observed in the solid phase by careful screening of the crystallization conditions. Further studies are needed to confirm this hypothesis. **3b**, having two *cis*-alkene moieties, is more thermodynamically stable than the corresponding all-*trans* and *cis*-*trans* isomers by 190 and 116 kJ mol^{-1}, respectively. Therefore, isomerization to these isomers is also unlikely.

The calculated strain energies of ene-[*N*]CPPs (N = 5-12) and (ene)$_2$-[*N*]CPPs (N = 5-12) suggest that the former are significantly more strained than the latter (Table 2). For example, the strain energies of **1b** and **3b** are 262 kJ mol^{-1} and 91 kJ mol^{-1}, respectively. These results are consistent with the trend of the out-of-plane bending angles of the paraphenylene unit observed both in the XRD analysis and the calculated structure. For **1b**, the strain is localized to ring C, with an *ipso* carbon deviating the most from planarity, which can be visualized by the method recently reported by Jasti and coworkers (Figure S7).[34] Despite the considerable strain of ene-[*N*]CPPs, they are less strained than [*N*]CPPs with similar sizes. For example, the strain energy of ene-[6]CPP (**1b**) is far smaller than that of [6]CPP (407 kJ mol^{-1}) and [7]CPP (357 kJ mol^{-1}),[22] suggesting that the twist does not induce strain in the cyclic structure.

To gain insights into the in-plane conjugation, the HOMO and LUMO energies of ene-[*N*]CPPs and (ene)$_2$-[*N*]CPPs were analyzed (Table 2 and Figure 4). The HOMO and LUMO energies of ene-[*N*]CPPs increase and decrease, respectively, as the number of paraphenylene units decreases (Figure 4, red lines). The same size dependency was previously reported for CPP,[22] and ene-[*N*]CPP is the second example of the opposite size dependency of normal Hückel molecules. On the other hand, the dependency of the HOMO and LUMO energies of (ene)$_2$-[*N*]CPPs on size is consistent with that of conventional Hückel molecules (Figure 4, blue lines).[22] The observed size dependency is consistent with the quinoidal contribution in **1** and **3**, in which **1** has a more significant quinoidal contribution than **3**.
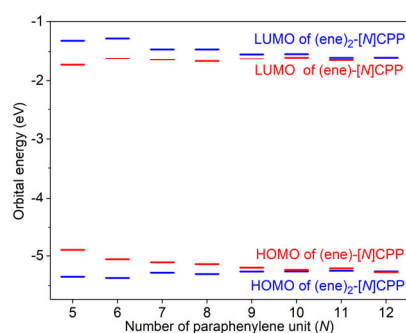

Figure 4. HOMO and LUMO energies of (ene)-[*N*]CPP and (ene)$_2$-[*N*]CPP calculated at the B3LYP/6-31G* level of theory.

Photophysical properties. The UV-vis absorption spectra of **1a-d** in CH$_2$Cl$_2$ are shown in Table 2 and Figure 5a. All compounds possess a strong absorption band (λ_2) at approximately 320-330 nm and a weak absorption band (λ_1) in the lower-energy region, and these bands are redshifted as the ring size decreases

($\lambda_{1(max)}$ = 416 nm for **1b**, 383 nm for **1c**, and 379 nm for **1d**). **1a** and **2** have absorption similar to that of **1b** (Figure S10).

Time-dependent (TD) DFT calculations suggest that λ_1 can be assigned to the HOMO-LUMO transition, and the observed size dependency is consistent with the size dependency of the HOMO-LUMO energies, as discussed above. The same trend was also observed for CPPs.[22, 35] λ_{abs2} can be assigned to the sum of the (HOMO-1)-LUMO and HOMO-(LUMO+1) transitions, and the insensitivity of the absorption to the size is also very similar to that observed in CPPs.[22] These results suggest that the size of the ring is the primary factor determining the absorption spectra, and that the in-plane conjugation of **1** and **2** is preserved in a solution phase despite the free rotation of the paraphenylene unit.
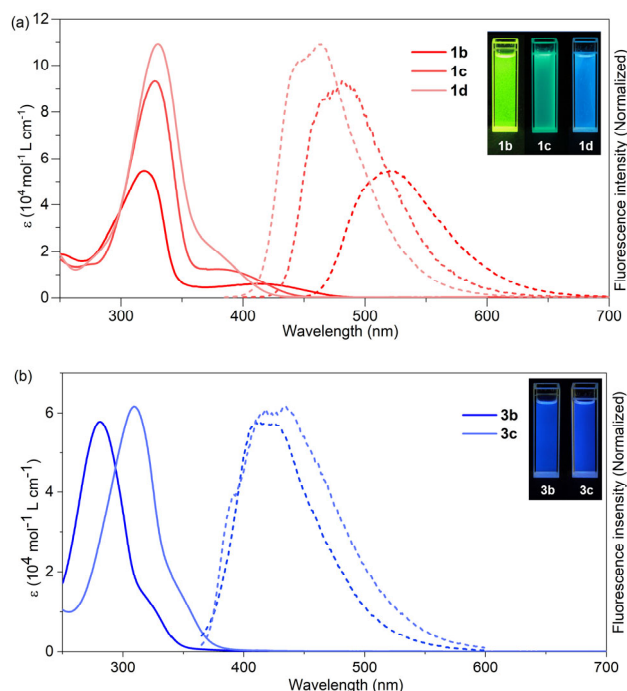

Figure 5. UV−vis absorption (solid line) and fluorescence (dashed line) spectra of (a) 1 and (b) 3 in CH$_2$Cl$_2$. Photographs in the insets show the fluorescence emission of the samples.

The absorption spectra of **3b** and **3c** also show two bands (Table 2 and Figure 6b): a strong band (λ_2) and a weak shoulder band (λ_1) in the high- and low-energy regions, respectively. λ_1 is assigned to the HOMO-LUMO transition, and λ_2 is assigned to the sum of the (HOMO-1)-LUMO and HOMO-(LUMO+1) transitions on the basis of the TD-DFT calculation. Interestingly, **3** has a different size dependency than **1**; both λ_1 and λ_2 are blueshifted as the ring size decreases. These results are also consistent with the size dependency of the HOMO-LUMO energy of (ene)$_2$-[*N*]CPPs.

Both **1a-d** and **3b-c** emit fluorescence with distinct size dependence, as observed in the absorption spectra (Table 2 and Figure 5); the fluorescence of **1** is redshifted as the ring size increases, while that of **3** is blueshifted. The Stokes shift observed for **3** is significantly smaller than that observed for **1**, probably due to slight structural relaxation at the excited state because **3** is less strained than **1**. The fluorescence quantum yields (Φ_F) increase as the ring size in both **1** and **3** increases, and the same trend was previously observed in the fluorescence of CPPs.[36]

Electrochemical properties. Next, the redox properties were investigated by using cyclic voltammetry (CV) and

differential pulse voltammetry (DPV) (Table 2, Figure 6, and Figure S11). The cyclic voltammograms of **1a-d** and **2** showed two or three oxidation waves with low reversibility, and those of **3b-c** exhibited one irreversible oxidation wave for samples in (CH₂Cl)₂. These results are in sharp contrast to those of [*n*]CPPs, which undergo reversible two-electron oxidation.[37] The first oxidation potentials of **1b-d** and **3b-c** exhibit opposite size dependencies; the potential of **1** increases and that of **3** decreases as the ring size decreases. These results are consistent with the size dependency of the HOMO energy of **1** and **3** (Table 2). The reversibility of the first oxidation wave of **1** increases as the ring size increases, as revealed by CV upon scanning only the first oxidation wave. These results suggest that the stability of radical cations increases with increasing ring size.
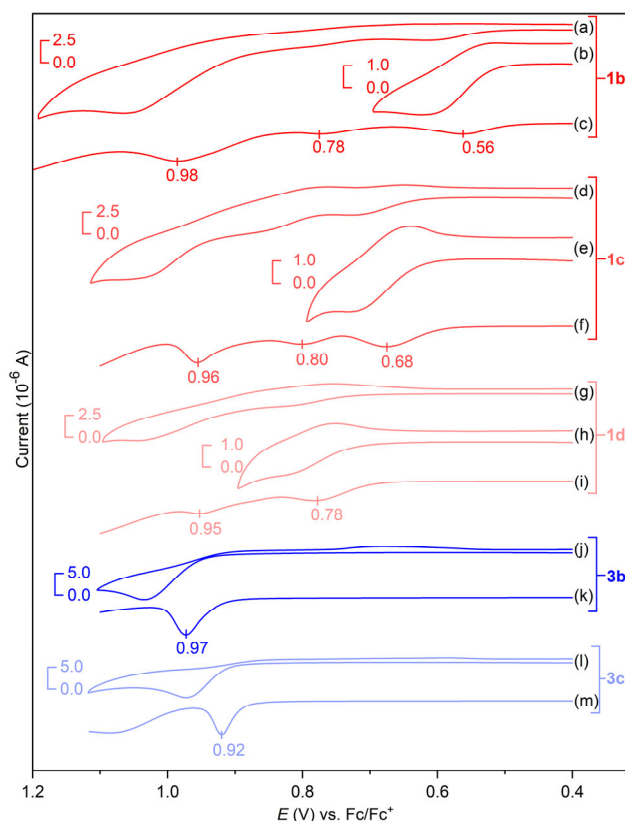

Figure 6. (a, d, g, j, l) Cyclic and (c, f, i, k, l) differential pulse voltammograms of 1b-d and 3b-c in Bu₄NPF₆/(CH₂Cl)₂ at room temperature; scan rate = 0.1 V s⁻¹. (b, e, h) Cyclic voltammograms of 1b-d upon scanning of the first oxidation wave.

Chemical oxidation. The chemical oxidation of **1** was next examined to elucidate the origin of the instability of the oxidized species. When **1b** in CH₂Cl₂ was treated with NOSbF₆ (1.0 equiv.) in CH₃CN at room temperature (Table 3, entry 1), the yellow solution of **1b** immediately turned green. The total consumption of **1b** was confirmed by UV-vis absorption spectra. Then, *i*-PrNEt₂ (2.0 equiv.) was added to quench the oxidized species. Two products, **13b** and **14b**, were isolated in 29% and 49% yields, respectively, and a small amount of **1b** was recovered (6%). The low recovery of **1b** was consistent with the observed low reversibility in the CV analysis. The MALDI-TOF MS spectra of **13b** and **14b** (*m/z* = 962.3935 and 1444.5890, respectively) revealed the formation of a dimer and a trimer of **1b**, respectively, with the loss of two hydrogens.

The same experiment was carried out for both **1c** and **1d** (entries 2 and 3). As the ring size increased, the recovery of **1** increased; 31% and 55% of **1c** and **d** was recovered, respectively. Additionally, the amount of trimer **14** was significantly decreased. These results are consistent with the increased reversibility observed in the CV measurements as the size of **1** increases.

The structure of dimer **13b** was unambiguously determined by XRD analysis; dimerization occurs at ring *C* of **1b**, accompanied by rearrangement from *para*- to *ortho*-substitution (Figure 7). As the ¹H NMR spectrum of **13c** is very similar to that of **13b**, **13c** most likely has the same rearranged structure. In contrast, several attempts to characterize **13d** and **14** were unsuccessful.

Table 3. Chemical oxidation of 1.
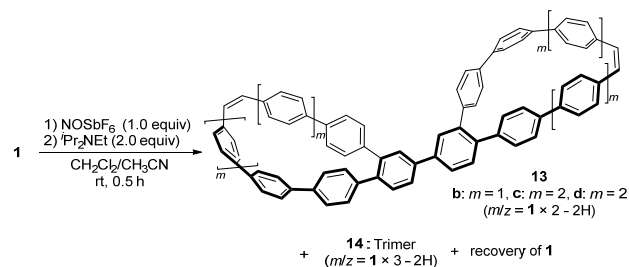
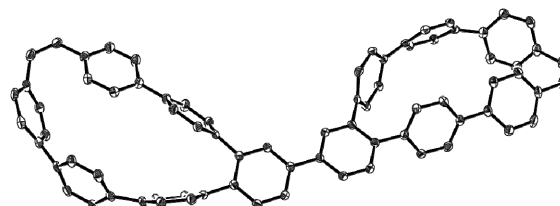| Entry	Substrate	Isolation yield		Recovery of **1** (%)ᵃ
		13 (%)	**14** (%)	
1	**1b**	**13b** (29)	**14b** (49)	**1b** (6)
2	**1c**	**13c** (24)	**14c** (8)	**1c** (31)
3	**1d**	**13d** (20)	**14d** (0)	**1d** (55)

Figure 7. X-ray crystal structure of 13b. Hydrogen atoms and solvents are omitted for clarity. The thermal ellipsoids are scaled at the 50% probability level.

A plausible mechanism for the formation of **13b-c** is illustrated in Figure 8. Upon formation of radical cation **1**ˑ⁺ by the single-electron oxidation of **1**, dimerization between the *ipso* carbon on the paraphenylene unit farthest from the alkene takes place, affording dimeric dication **15**. Then, **15** undergoes twofold 1,2-aryl rearrangement at the cationic paraphenylene unit, yielding **16**, which is further rearranged to **17**. The elimination of protons from **17** affords **13**. The driving force of the reaction is the relief of strain, and DFT calculations suggested that both transformations from **15** to **16** and from **16** to **17** are exothermic, with formation enthalpies of –6.5 kJ mol⁻¹ and -57 kJ mol⁻¹, respectively.

The DFT calculation of **1**ˑ⁺ suggested that the spin density is relatively localized on the ipso carbons of the farthest paraphenylene unit, probably because these carbons have significant *sp*³-carbon character, judging from the out-of-plane bending angles of the neutral state (Figure 9). Therefore, the coupling reaction takes place kinetically at this paraphenylene unit.

The calculations also suggest that the radical cations have a more quinoidal contribution than the neutral compounds, judging from the BLA values of the paraphenylene units. The same trend was also observed for CPP.[38]
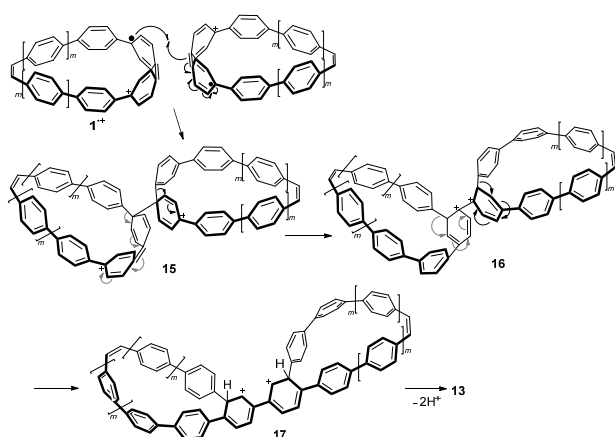
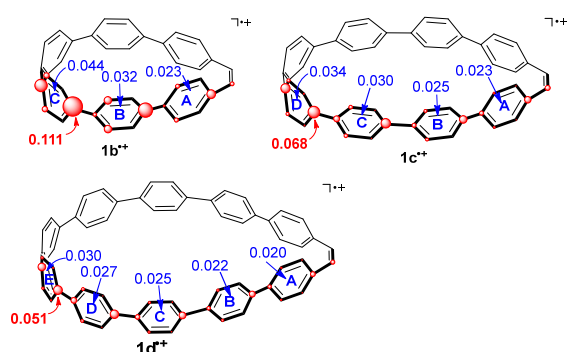**Figure 8. A plausible mechanism for the formation of 13.**

Figure 9. The selected Mulliken spin density and BLA values of the radical cation 1b-d·⁺ determined by DFT calculations at the UB3LYP/6-31G* level of theory. The spin density is indicated on carbon atoms as red circles, the size of which corresponds to the relative magnitude of the spin density. The BLA values of the paraphenylene unit are shown in blue.

In summary, CPPs with Möbius topology, (ene)- and phe-CPPs, were synthesized by inserting alkene or *ortho*-phenylene units into a CPP skeleton. Despite the presence of a twist, (ene)-CPPs are in-plane conjugated and possess unique size dependence, i.e., the opposite size dependency of the HOMO-LUMO energy relative to normal π-conjugated molecules. Furthermore, this unique feature is experimentally confirmed by absorption and emission spectra and electrochemical oxidation. These results suggest a new design and synthetic method for cyclic π-conjugated molecules with various topologies and properties.

ASSOCIATED CONTENT

Supporting Information. The Supporting Information is available free of charge via the Internet at http://pubs.acs.org." Full details of experimental procedures, characterization data, NMR spectra, and computational details (PDF)

Accession Codes
CCDC 2080799-2080805 contain the supplementary crystallographic data for this paper. These data can be obtained free of charge via www.ccdc.cam.ac.uk/data_request/cif, or by emailing data_request@ccdc.cam.ac.uk, or by contacting The Cambridge Crystallographic Data Centre, 12 Union Road, Cambridge CB2 1EZ, UK; fax: +44 1223 336033.

AUTHOR INFORMATION

Corresponding Author
Eiichi Kayahara − Institute for Chemical Research, Kyoto University, Uji 611-0011, Japan; orcid.org/0000-0003-1663-5273; Email: kayahara@scl.kyoto-u.ac.jp
Shigeru Yamago − Institute for Chemical Research, Kyoto University, Uji 611-0011, Japan; orcid.org/0000-0002-4112-7249; Email: yamago@scl.kyoto-u.ac.jp

Authors
Tomoaki Terabayashi − Institute for Chemical Research, Kyoto University, Uji 611-0011, Japan
Tohru Nishinaga − Department of Chemistry, Tokyo Metropolitan University, Hachioji, Tokyo 192-0397, Japan; orcid.org/0000-0002-9081-3659
Tatsuhisa Kato − Institute for Chemical Research, Kyoto University, Uji 611-0011, Japan; orcid.org/0000-0003-0032-8535
Yoshiyuki Mizuhata − Institute for Chemical Research, Kyoto University, Uji 611-0011, Japan; orcid.org/0000-0001-5301-0024
Norihiro Tokitoh − Institute for Chemical Research, Kyoto University, Uji 611-0011, Japan; orcid.org/0000-0003-1083-7245

Notes
The authors declare no competing financial interest.

REFERENCES
(1) Kroto, H. W.; Heath, J. R.; O'Brien, S. C.; Curl, R. F.; Smalley, R. E. C₆₀: Buckminsterfullerene. *Nature* **1985**, *318*, 162-163.
(2) Iijima, S. Helical microtubules of graphitic carbon. *Nature* **1991**, *354*, 56-58.
(3) Scott, L. T.; Petrukhina, M. A. Fragments of Fullerenes and Carbon Nanotubes: Designed Synthesis, Unusual Reactions, and Coordination Chemistry. John Wiley & Sons: Hobboken, New Jersey, 2011.
(4) Ajami, D.; Oeckler, O.; Simon, A.; Herges, R. Synthesis of a Möbius aromatic hydrocarbon. *Nature* **2003**, *426*, 819.
(5) Herges, R. Topology in Chemistry: Designing Möbius Molecules. *Chem. Rev.* **2006**, *106*, 4820-4842.
(6) Stępień, M.; Latos-Grażyński, L.; Sprutta, N.; Chwalisz, P.; Szterenberg, L. Expanded Porphyrin with a Split Personality: A Hückel–Möbius Aromaticity Switch. *Angew. Chem. Int. Ed.* **2007**, *46*, 7869-7873.
(7) Tanaka, Y.; Saito, S.; Mori, S.; Aratani, N.; Shinokubo, H.; Shibata, N.; Higuchi, Y.; Yoon, Z. S.; Kim, K. S.; Noh, S. B.; Park, J. K.; Kim, D.; Osuka, A. Metalation of Expanded Porphyrins: A Chemical Trigger Used To Produce Molecular Twisting and Möbius Aromaticity. *Angew. Chem. Int. Ed.* **2008**, *47*, 681-684.
(8) Shin, J.-Y.; Kim, K. S.; Yoon, M.-C.; Lim, J. M.; Yoon, Z. S.; Osuka, A.; Kim, D. Aromaticity and photophysical properties of various topology-controlled expanded porphyrins. *Chem. Soc. Rev.* **2010**, *39*, 2751-2767.
(9) Tanaka, T.; Osuka, A. Chemistry of meso-Aryl-Substituted Expanded Porphyrins: Aromaticity and Molecular Twist. *Chem. Rev.* **2017**, *117*, 2584-2640.
(10) Schaller, G. R.; Topić, F.; Rissanen, K.; Okamoto, Y.; Shen, J.; Herges, R. Design and synthesis of the first triply twisted Möbius annulene. *Nat. Chem.* **2014**, *6*, 608-613.
(11) Naulet, G.; Sturm, L.; Robert, A.; Dechambenoit, P.; Röhricht, F.; Herges, R. Bock, H.; Durola, F. Cyclic tris-[5]helicenes with single and triple twisted Möbius topologies and Möbius aromaticity. *Chem. Sci.* **2018**, *9*, 8930-8936.

(12) Li, Y.; Yagi, A.; Itami, K. Synthesis of Highly Twisted, Nonplanar Aromatic Macrocycles Enabled by an Axially Chiral 4,5-Diphenylphenanthrene Building Block. *J. Am. Chem. Soc.* **2020**, *142*, 3246-3253.

(13) Golder, M. R.; Jasti, R. Syntheses of the Smallest Carbon Nanohoops and the Emergence of Unique Physical Phenomena. *Acc. Chem. Res.* **2015**, *48*, 557-566.

(14) Omachi, H.; Segawa, Y.; Itami, K. Synthesis of Cycloparaphenylenes and Related Carbon Nanorings: A Step toward the Controlled Synthesis of Carbon Nanotubes. *Acc. Chem. Res.* **2012**, *45*, 1378-1389.

(15) Yamago, S.; Kayahara, E.; Iwamoto, T. Organoplatinum-Mediated Synthesis of Cyclic π-Conjugated Molecules: Towards a NewOrga of Three-Dimensional Aromatic Compounds. *Chem. Rec.* **2014**, *14*, 84-100.

(16) Lovell, T. C.; Colwell, C. E.; Zakharov, Lev N.; Jasti, R. Symmetry breaking and the turn-on fluorescence of small, highly strained carbon nanohoops. *Chem. Sci.* **2019**, *10*, 3786-3790.

(17) Li, P.; Zakharov, L. N.; Jasti, R. A Molecular Propeller with Three Nanohoop Blades: Synthesis, Characterization, and Solid-State Packing. *Angew. Chem. Int. Ed.* **2017**, *56*, 5237-5241.

(18) Sisto, T. J.; Zakharov, L. N.; White, B. M.; Jasti, R. Towards pi-extended cycloparaphenylenes as seeds for CNT growth: investigating strain relieving ring-openings and rearrangements. *Chem. Sci.* **2016**, *7*, 3681-3688.

(19) Nishigaki, S.; Shibata, Y.; Nakajima, A.; Okajima, H.; Masumoto, Y.; Osawa, T.; Muranaka, A.; Sugiyama, H.; Horikawa, A.; Uekusa, H.; Koshino, H.; Uchiyama, M.; Sakamoto, A.; Tanaka, K. Synthesis of Belt- and Möbius-Shaped Cycloparaphenylenes by Rhodium-Catalyzed Alkyne Cyclotrimerization. *J. Am. Chem. Soc.* **2019**, *141*, 14955-14960.

(20) Senthilkumar, K.; Kondratowicz, M.; Lis, T.; Chmielewski, P. J.; Cybińska, J.; Zafra, J. L.; Casado, J.; Vives, T.; Crassous, J.; Favereau, L.; Stępień, M., Lemniscular [16]Cycloparaphenylene: A Radially Conjugated Figure-Eight Aromatic Molecule. *J. Am. Chem. Soc.* **2019**, *141*, 7421-7427.

(21) Schaub, T. A.; Prantl, E. A.; Kohn, J.; Bursch, M.; Marshall, C. R.; Leonhardt, E. J.; Lovell, T. C.; Zakharov, L. N.; Brozek, C. K.; Waldvogel, S. R.; Grimme, S.; Jasti, R. Exploration of the Solid-State Sorption Properties of Shape-Persistent Macrocyclic Nanocarbons as Bulk Materials and Small Aggregates. *J. Am. Chem. Soc.* **2020**, *142*, 8763-8775.

(22) Iwamoto, T.; Watanabe, Y.; Sakamoto, Y.; Suzuki, T.; Yamago, S. Selective and Random Syntheses of [n]Cycloparaphenylenes (n = 8-13) and Size Dependence of Their Electronic Properties. *J. Am. Chem. Soc.* **2011**, *133*, 8354-8361.

(23) Ishiyama, T.; Matsuda, N.; Miyaura, N.; Suzuki, A. Platinum(0)-catalyzed diboration of alkynes. *J. Am. Chem. Soc.* **1993**, *115*, 11018-11019.

(24) Patel, V. K.; Kayahara, E.; Yamago, S. Practical Synthesis of [n]Cycloparaphenylenes (n=5, 7–12) by H_2SnCl_4-Mediated Aromatization of 1,4-Dihydroxycyclo-2,5-diene Precursors. *Chem. Eur. J.* **2015**, *21*, 5742-5749.

(25) Cheung, K. Y.; Chan, C. K.; Liu, Z.; Miao, Q. A Twisted Nanographene Consisting of 96 Carbon Atoms. *Angew. Chem. Int. Ed.* **2017**, *56*, 9003-9007.

(26) Yamago, S.; Watanabe, Y.; Iwamoto, T. Synthesis of [8]Cycloparaphenylene from a Square-Shaped Tetranuclear Platinum Complex. *Angew. Chem. Int. Ed.* **2010**, *49*, 757-759.

(27) Evans, P. J.; Darzi, E. R.; Jasti, R. Efficient room-temperature synthesis of a highly strained carbon nanohoop fragment of buckminsterfullerene. *Nat. Chem.* **2014**, *6*, 404-408.

(28) Xia, J.; Jasti, R. Synthesis, Characterization, and Crystal Structure of [6]Cycloparaphenylene. *Angew. Chem. Int. Ed.* **2012**, *51*, 2474-2476.

(29) Sisto, T. J.; Golder, M. R.; Hirst, E. S.; Jasti, R. Selective Synthesis of Strained [7]Cycloparaphenylene: An Orange-Emitting Fluorophore. *J. Am. Chem. Soc.* **2011**, *133*, 15800-15802.

(30) Xia, J.; Bacon, J. W.; Jasti, R. Gram-scale synthesis and crystal structures of [8]- and [10]CPP, and the solid-state structure of C60@[10]CPP. *Chem. Sci.* **2012**, *3*, 3018-3021.

(31) Fujitsuka, M.; Iwamoto, T.; Kayahara, E.; Yamago, S.; Majima, T. Enhancement of the Quinoidal Character for Smaller [n]Cycloparaphenylenes Probed by Raman Spectroscopy. *ChemPhysChem* **2013**, *14*, 1570-1572.

(32) Fincher, C. R.; Chen, C. E.; Heeger, A. J.; MacDiarmid, A. G.; Hastings, J. B. Structural Determination of the Symmetry-Breaking Parameter in *trans*-(CH)$_x$. *Phys. Rev. Lett.* **1982**, *48*, 100-104.

(33) Chien, J. C. W.; Karasz, F. E.; Shimamura, K. An estimate of bond length alternation in trans-polyacetylene. *Macromol. Rapid Commun.* **1982**, *3*, 655-659.

(34) Colwell, C. E.; Price, T. W.; Stauch, T.; Jasti, R. Strain visualization for strained macrocycles. *Chem. Sci.* **2020**, *11*, 3923-3930.

(35) Segawa, Y.; Fukazawa, A.; Matsuura, S.; Omachi, H.; Yamaguchi, S.; Irle, S.; Itami, K. Combined experimental and theoretical studies on the photophysical properties of cycloparaphenylenes. *Org. Biomol. Chem.* **2012**, *10*, 5979-5984.

(36) Fujitsuka, M.; Cho, D. W.; Iwamoto, T.; Yamago, S.; Majima, T. Size-dependent fluorescence properties of [n]cycloparaphenylenes (n = 8-13), hoop-shaped π-conjugated molecules. *Phys. Chem. Chem. Phys.* **2012**, *14*, 14585-14588.

(37) Kayahara, E.; Fukayama, K.; Nishinaga, T.; Yamago, S. Size Dependence of [n]Cycloparaphenylenes (n=5–12) in Electrochemical Oxidation. *Chem. Asian J.* **2016**, *11*, 1793-1797.

(38) Kayahara, E.; Kouyama, T.; Kato, T.; Takaya, H.; Yasuda, N.; Yamago, S. Isolation and Characterization of the Cycloparaphenylene Radical Cation and Dication. *Angew. Chem. Int. Ed.* **2013**, *52*, 13722-13726.

[*N*]Cycloparaphenylene
"Hückel"

"Möbius"

"Hückel"